Efficient calculation of the effective single-particle potential and its application in electron microscopy

Wei L. Wang and Efthimios Kaxiras

Department of Physics and School of Engineering and Applied Sciences, Harvard University, Cambridge, Massachusetts 02138, USA

We present an efficient method for obtaining the effective single-particle potential for electrons within density functional theory (DFT). In contrast to the independent atom model (IAM) often used to interpret microscopy experiments, our method includes the contributions from charge redistribution and exchange-correlation interactions in a realistic system. The method allows calculation of the effective potential through the widely used pseudopotential formalism instead of the costly all-electron calculations. A transferable and spin-independent core potential for each element is calculated once and for all. The nonlinear exchange-correlation interaction is treated explicitly. This scheme can be readily implemented in pseudopotential DFT codes. We demonstrate the usefulness of our method by calculating the scattering potential and simulating images of nitrogen point defects in graphene for transmission electron microscopy (TEM). The results are in good agreement with experiments.

Calculating the effective single-particle potential for electrons as a spatially dependent function in a condensed-matter system can be crucial in interpreting experimental results and predicting functional properties of the system. For example, the profile of a potential barrier across a tunneling junction has been used to estimate the spin injection rate.[1] Another broad field of applications is phase-contrast imaging in transmission electron microscopy (TEM),[2,3] where the effective single-particle potential projected along the electron beam direction determines the phase shift of the probing electron wave and thus affects the propagation of the wave and the formation of images.

The effective single-particle potential can be obtained with various levels of approximation in realistic quantum-mechanical calculations. Among them density functional theory[4,5] (DFT) is one of the most widely used tools. For reasons of efficiency, most DFT calculations are carried out using pseudopotentials[6–8] which have components that are orbital dependent. As a result, the potential used, particularly in the core region, is nonphysical and direct recovery of the realistic potential from the pseudovalence charge and the pseudopotential is not straightforward. Alternatively, all the electrons, including core electrons, can be explicitly treated in DFT calculations without pseudopotentials, in which case the potential, including that of the core region, can be trivially obtained. All-electron calculations are very expensive because the computational cost generally scales as $O(N^3)$, and treatment of the core wave functions is computationally difficult due to their finely spaced features. In this paper, we implement a procedure to recover the correct total potential in all regions by computing a core-potential correction once and for all, and applying it to routine pseudopotential DFT calculations. The core charge density is transferable and the potential contributed by nonlinear exchange correlation is treated in the manner introduced by Louie and Cohen.[9] This scheme is very efficient and can be straightforwardly implemented in existing DFT codes that compute the valence charge density. We show that simulations based on this method produce results that are in good agreement with experiments and all-electron calculations.

We start with the definition of the effective single-particle potential which is the derivative of the system energy with respect to an infinitesimal test charge localized at $\vec{r}$. We treat the test charge as a perturbation to the system, which is consistent with many relevant physical processes such as phase contrast imaging in TEM where the cross section for electron scattering is small and the inelastic scattering is negligible. The local potential of the system in the ground state is a functional of electron density $\rho(\vec{r})$ and spin polarization $\xi(\vec{r})$,

$$
\begin{aligned}
V_{\text{tot}}&[\rho(\mathbf{r}),\xi(\mathbf{r})](\mathbf{r},\sigma)\\
&= V_N(\mathbf{r}) + V_{ee}[\rho(\mathbf{r}),\xi(\mathbf{r})](\mathbf{r},\sigma)\\
&= V_N(\mathbf{r}) + V_H[\rho(\mathbf{r})](\mathbf{r}) + V_{xc}[\rho(\mathbf{r}),\xi(\mathbf{r})](\mathbf{r},\sigma),
\end{aligned} \quad (1)
$$

where $\sigma = +$ or $-$ for spin up or down. The normalized spin polarization is defined as

$$
\xi(\mathbf{r}) = \frac{\rho_+^v(\mathbf{r}) - \rho_-^v(\mathbf{r})}{\rho^v(\mathbf{r}) + \rho^c(\mathbf{r})}, \quad (2)
$$

where the ρ_+^v and ρ_-^v are respectively the spin-up and spin-down portion of the total valence electron density ρ^v, and ρ^c is the core electron density. The potential $V_N(\mathbf{r})$ contributed by a nucleus charge with Q_N at position R_N and the mean-field electron-electron interaction $V_H[\rho(\mathbf{r})](\mathbf{r})$ (Hartree term) are given by

$$
V_N(\mathbf{r}) = \frac{Q_N}{|\mathbf{r} - \mathbf{R}_N|} \quad (3)
$$

and

$$
V_H[\rho(\mathbf{r})](\mathbf{r}) = \int \frac{\rho(\mathbf{r}')}{|\mathbf{r}' - \mathbf{r}|} d^3 r'. \quad (4)
$$

The last functional in Eq. (1) accounts for the many-body exchange-correlation interactions the exact form of which is unknown. As an approximation, we adopt the same form of exchange-correlation functional for the fictitious single particles as in the Kohn-Sham ansatz:

$$
V_{xc}[\rho] = V_{xc}^{KS}[\rho], \quad (5)
$$

which can be a either a local or a nonlocal functional. The Hartree term is linear in the density ρ, and therefore we can

separate the contributions from the valence electrons:

$$V_H[\rho] = V_H[\rho^c] + V_H[\rho^v]. \tag{6}$$

Because of this linearity, we replace the actual valence density by a pseudovalence density $\tilde{\rho}^v$:

$$V_H[\rho] = \{V_H[\rho] - V_H[\tilde{\rho}^v]\} + V_H[\tilde{\rho}^v], \tag{7}$$

where we assume that $\{V_H[\rho] - V_H[\tilde{\rho}^v]\}$ is confined to the core region and is transferable. This assumption is consistent with the basis of any pseudopotential DFT calculations. We therefore obtain this term once and for all from atomic calculations using all the electrons for the total charge and using pseudopotentials for the pseudovalence charge, that is

$$V_H[\rho] = \{V_H[\rho_0] - V_H[\tilde{\rho}_0{}^v]\} + V_H[\tilde{\rho}^v], \tag{8}$$

where the subscript "0" donates quantities from all-electron calculations of single atoms. Note that the first term on the right-hand side of Eq. (8) includes the potential correction not only from core orbitals but also from the difference in the core region between real-valence orbitals and pseudovalence orbitals.

The exchange-correlation term is nonlinear and cannot be separately and accurately calculated.[9] Instead, the core charge has to be calculated and passed to the pseudopotential calculation, and then summed with the density of pseudovalence electrons:

$$V_{xc}[\rho] = V_{xc}^{KS}[\rho^c + \rho^v, \xi], \tag{9}$$

$$V_{xc}[\rho] = V_{xc}^{KS}[(\rho^c + \rho^v - \tilde{\rho}^v) + \tilde{\rho}^v, \xi]. \tag{10}$$

Again, the transferable core charge $\rho^c + \rho^v - \tilde{\rho}^v$ is obtained from single-atom calculations, giving

$$V_{xc}[\rho] = V_{xc}^{KS}[(\rho_0 - \tilde{\rho}_0{}^v) + \tilde{\rho}^v, \xi]. \tag{11}$$

Our scheme also fits in the framework of the projector augmented-wave (PAW) method[10] except that we wrap together the potential term due to the core and that due to the difference of the partial waves and the smooth partial waves, and calculate it in a single numerical step. The implementation of our scheme is straightforward in existing DFT code such as SIESTA.[11] The transferable core potential can be calculated as follows: First, an atomic calculation is carried out using all the electrons, which gives the potential as a function of distance from the nucleus. The next atomic calculation uses a pseudopotential and the pseudovalence potential is obtained. The pseudovalence potential and the entire exchange-correlation potential is then subtracted from the atomic potential, providing a core-correction potential that is transferable and spin independent. The core-correction potential is saved and added to routine pseudopotential DFT calculations where the pseudovalence potential and the entire exchange-correlation potential with full or partial core correction[9] is calculated in a standard way.[11]

This formulation in principle can be used whenever a realistic effective single-particle potential is of interest. In particular, it applies to high-resolution electron microscopy. With the recent breakthrough of abberation correction and improvement on the electron probe energy resolution,[12,13] the role of high resolution and energy resolved electron microscopy is becoming more important in discovering and characterizing new materials such as carbon allotropes.[14–16] In phase contrast TEM imaging, a sample can be considered as a weak scatterer potential field which modifies the phase of incoming electron plane waves. The process is mainly elastic and the image contrast is formed by wave reconstruction after the modification introduced by the sample potential field and the manipulation of the electron optics. Conventionally simulations are carried out based on the so-called independent atomic model[2,17] in which individual atomic potentials are superimposed in a system to account for the total potential. Obviously all bonding effects are lost in this approximation. Recent experiments and simulations[18] showed that charge redistribution due to bonding plays a significant role in imaging, as for example, in the substitutional defect in graphene, where realistic first-principles methods are required to explain the experimental results. Although all electron calculations can be used, the cost is high, which motivated our implementation of the above method to calculate the scattering potential efficiently. We show below that simulations based on our method reproduce the experimental results very well. We further show the effects of imaging conditions on image features that were experimentally detected.

To illustrate the efficiency and accuracy of our method, we simulate a single nitrogen substitutional defect in graphene.[18–23] The charge is redistributed significantly in the vicinity of the nitrogen because of the difference in chemical potential, which alters the screened potential, rendering the defect visible in TEM images under favorable imaging conditions. We calculated the projected effective single-particle potential using the method described above. The substitutional defect in graphene is first relaxed using a conjugate gradient algorithm in a supercell until the magnitude of forces on all atoms is smaller than 0.04 eV/Å. The generalized gradient approximation (GGA) exchange-correlation density functional PBE (Perdew, Burke, and Ernzerhof)[24] was employed together with a double-ζ plus polarization basis set, and a mesh cutoff of 200 Ry in the SIESTA code. The effective single-particle potential is obtained and projected along the direction perpendicular to the basal plane of graphene to obtain the projected potential $V_s(\mathbf{x})$, where $\mathbf{x}$ is a two-dimensional (2D) position vector in the basal plane. Based on this scattering potential, the TEM image is simulated within the weak phase object approximation[2] in which the incident plane wave in the z direction $\psi_i(\mathbf{x})$ is phase shifted by the calculated effective potential V_s, so that the transmission wave is

$$\psi_t(\mathbf{x}) = \psi_i(\mathbf{x})\exp[SV_s(\mathbf{x})z]. \tag{12}$$

The interaction parameter $S = 2\pi me\lambda/h^2$, where m is the relativistic mass of electrons at 80 kV. e and λ are the charge and wavelength of electrons, respectively. The effect of the calculated potential on the TEM image contrast $g(\mathbf{x})$
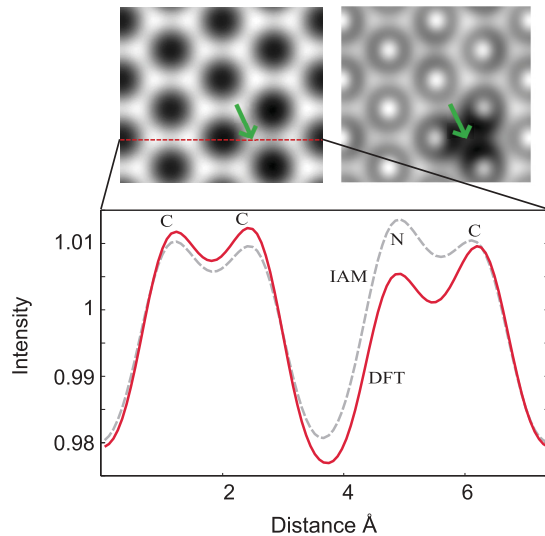
FIG. 1. (Color online) Simulated TEM image contrast profile of N substitutional defect in graphene. The top-left image shows the TEM phase contrast of graphene with a N substitutional defect pointed by the green arrow, simulated using our method. The image on the right makes the N defect more visible by removing the graphene lattice using a Fourier filter. A profile along the red dashed line that goes through the center of both C-C and N-C bonds is shown in the bottom panel. The reduced intensity shown on N and the C atom to which it is bonded reproduce the features shown in experiment (Ref. 18). The phase contrast image was simulated with spherical abberation $C_s = 20$ μm and defocus $df = 15.5$ nm. As a comparison, the contrast profile from the simulation based on IAM is shown by the dashed line.

is calculated through a point spread function $h(\mathbf{x})$ which is determined by the electronic optics of the TEM,

$$g(\mathbf{x}) = 1 + 2SV_z(\mathbf{x}) \otimes h(\mathbf{x}). \qquad (13)$$

The TEM image is shown in the inset of Fig. 1 for spherical abberation $C_s = 20$ μm, matching the condition in the experiment.[18] The profile cutting through both N and C atoms as well as the C-C and N-C bonds is plotted in Fig. 1. The reduced intensity at the N atom and its nearest C neighbor, by 20% and 9% respectively at defocus 15.5 nm, reproduce the defect features that were observed in the experiment.[18] These features are not seen in a similar simulation that is based on the independent atom model (IAM) scattering potential in which the intensity on the N site is slightly increased instead.

We further explore the effects of defocus on the image contrast. Figure 2 shows the intensity ratio, defined as the intensity of the N atom and its nearest neighbor carbon over that of other carbon atoms, as a function of defocus. It is clear that the defect feature is highly visible when the defocus gets close to 15 nm but quickly diminishes as the defocus moves away form this critical value. On the other hand, the image contrast diminishes when approaching 15 nm, which could be overwhelmed by the noise floor; it is important to optimize defocus to balance both effects. In TEM practice, the setting of the precise value of defocus is difficult due to imperfect calibration, drift, and noise, and one needs to move the defocus
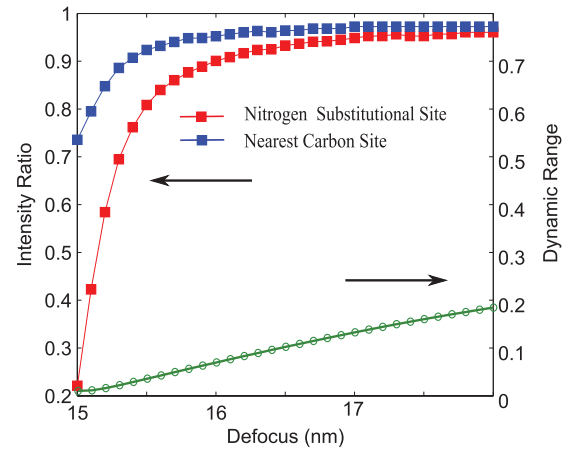

FIG. 2. (Color online) Variation of the contrast of the nitrogen defect feature graphene with defocus. The image feature, observed as reduced intensity of the N substitutional defect (red line) and the C atom to which it is bonded (blue line), becomes prominent when defocus approaches 15 nm from larger values and is quickly reduced when the defocus increases. The dynamic range of the image (right axis) diminishes when defocus approaches 15 nm. The intensity ratio is given relative to its value at a C site far from the N defect. The dynamic range (green line) is the range of the image intensity as a fraction of the electron beam illumination.

into the expected range and carefully adjust to obtain a good image of the feature. It is also important to minimize the drift and noise in the TEM to stabilize the image while acquiring the data.

We also varied the value of spherical abberation C_s in our simulation. The visibility of the defect features and the sensitivity to defocus does not change much with further improved abberation correction. This makes physical sense because the change of the potential profile due to the defect is a smooth function on the scale of the lattice. Further improvement of the information limit beyond the lattice frequency does not improve the resolution of the defect features. In other cases when fine details in the image contrast are of importance beyond the lattice frequency,[25] further reduction of C_s could be useful for quantitative characterization. Therefore, the importance of using the effective potential calculated by our method instead of the IAM potential could be relevant for a wide range of C_s values.

In summary, we have proposed and implemented a method to obtain the accurate effective single-particle potential using standard pseudopotential DFT calculations with a small additional cost of a transferable core-potential correction. The method can be straightforwardly implemented to existing pseudopotential DFT codes and applied efficiently to large systems. The method was tested in TEM image simulations where bonding effects are significant and the results are in good agreement with experiments.

[1] L. E. Hueso, J. M. Pruneda, V. Ferrari, G. Burnell, J. P. Valdes-Herrera, B. D. Simons, P. B. Littlewood, E. Artacho, A. Fert, and N. D. Mathur, Nature (London) **445**, 410 (2007).

[2] E. J. Kirkland, *Advanced Computing in Electron Microscopy* (Springer, 2010).

[3] D. B. Williams, and C. B. Carter, *Transmission Electron Microscopy: A Textbook for Materials Science* (Plenum, New York, 1996).

[4] P. Hohenberg and W. Kohn, Phys. Rev. **136**, B864 (1964).

[5] W. Kohn and L. J. Sham, Phys. Rev. **140**, A1133 (1965).

[6] M. L. Cohen, Phys. Today **32**(6), 40 (1979).

[7] M. T. Yin and M. L. Cohen, Phys. Rev. Lett. **45**, 1004 (1980).

[8] M. L. Cohen, Annu. Rev. Mater. Sci. **14**, 119 (1984).

[9] S. G. Louie, S. Froyen, and M. L. Cohen, Phys. Rev. B **26**, 1738 (1982).

[10] P. E. Blochl, Phys. Rev. B **50**, 17953 (1994).

[11] J. M. Soler, E. Artacho, J. D. Gale, A. Garcia, J. Junquera, P. Ordejon, and D. Sanchez-Portal, J. Phys.: Condens. Matter **14**, 2745 (2002).

[12] S. J. Pennycook, M. Varela, C. J. D. Hetherington, and A. I. Kirkland, MRS Bull. **31**, 36 (2006).

[13] D. J. Smith, Microsc. Microanal. **14**, 2 (2008).

[14] A. Hashimoto, K. Suenaga, A. Gloter, K. Urita, and S. Iijima, Nature (London) **430**, 870 (2004).

[15] J. C. Meyer, A. K. Geim, M. I. Katsnelson, K. S. Novoselov, T. J. Booth, and S. Roth, Nature (London) **446**, 60 (2007).

[16] J. C. Meyer, C. O. Girit, M. F. Crommie, and A. Zettl, Nature (London) **454**, 319 (2008).

[17] B. L. Jhanwar, S. P. Khare, and M. K. Sharma, Phys. Rev. A **22**, 2451 (1980).

[18] J. C. Meyer, S. Kurasch, H. J. Park, V. Skakalova, D. Kunzel, A. Gross, A. Chuvilin, G. Algara-Siller, S. Roth, T. Iwasaki, U. Starke, J. H. Smet, and U. Kaiser, Nat. Mater. **10**, 209 (2011).

[19] L. Y. Zhao, R. He, K. T. Rim, T. Schiros, K. S. Kim, H. Zhou, C. Gutierrez, S. P. Chockalingam, C. J. Arguello, L. Palova, D. Nordlund, M. S. Hybertsen, D. R. Reichman, T. F. Heinz, P. Kim, A. Pinczuk, G. W. Flynn, and A. N. Pasupathy, Science **333**, 999 (2011).

[20] G. P. Dai, J. M. Zhang, and S. G. Deng, Chem. Phys. Lett. **516**, 212 (2011).

[21] D. Usachov, O. Vilkov, A. Gruneis, D. Haberer, A. Fedorov, V. K. Adamchuk, A. B. Preobrajenski, P. Dudin, A. Barinov, M. Oehzelt, C. Laubschat, and D. V. Vyalikh, Nano Lett. **11**, 5401 (2011).

[22] H. B. Wang, T. Maiyalagan, and X. Wang, ACS Catal. **2**, 781 (2012).

[23] S. Park, Y. C. Hu, J. O. Hwang, E. S. Lee, L. B. Casabianca, W. W. Cai, J. R. Potts, H. W. Ha, S. S. Chen, J. Oh, S. O. Kim, Y. H. Kim, Y. Ishii, and R. S. Ruoff, Nat. Commun. **3**, 638 (2012).

[24] J. P. Perdew, K. Burke, and M. Ernzerhof, Phys. Rev. Lett. **77**, 3865 (1996).

[25] W. L. Wang, S. Bhandari, W. Yi, D. C. Bell, R. Westervelt, and E. Kaxiras, Nano Lett. **12**, 2278 (2012).